The following Communications have been judged by at least two referees to be "very important papers" and will be published online at www.angewandte.org soon:

Author Profile

Books

Highlights

Homogeneous Catalysis

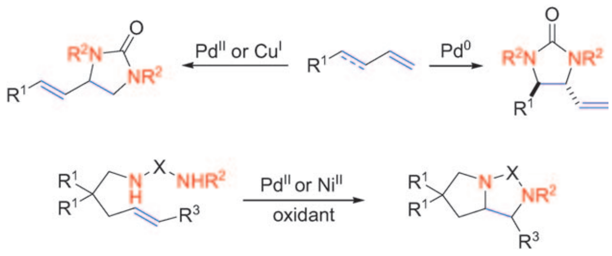

Diaminations are a girl's best friend: New reactions in the field of transition-metal-catalyzed diamination of olefins provide a powerful tool for the elaboration of more complex molecules bearing the 1,2-diamine moiety. An overview of these methods, including asymmetric versions, is given.

Scaffold Synthesis

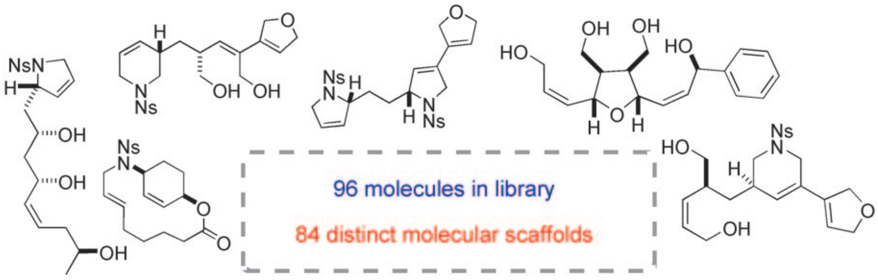

Building a better library: The synthesis of a library of natural-product-like small molecules with unprecedented scaffold diversity has been reported (see scheme; Ns = nosylate). The library represents a significant advancement in the capability of synthetic chemists to generate structurally diverse and complex small molecules in a rapid manner.

Reviews

Theoretical Chemistry

H. M. Senn,* W. Thiel* ____ **1198 – 1229**

QM/MM Methods for Biomolecular Systems

Two are better than one: Quantum mechanics/molecular mechanics (QM/MM) methods are the state-of-the-art computational technique for treating reactive and other “electronic” processes in biomolecular systems. This Review presents the general methodological aspects of the QM/MM approach, its use within optimization and simulation techniques, and its areas of application, always with a biomolecular focus.

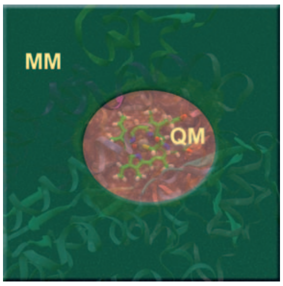

Communications

Inorganic Nanotubes

R. Kreizman, S. Y. Hong, J. Sloan, R. Popovitz-Biro A. Albu-Yaron, G. Tobias, B. Ballesteros, B. G. Davis, M. L. H. Green, R. Tenne* __ **1230 – 1233**

Core–Shell PbI_2@WS_2 Inorganic Nanotubes from Capillary Wetting

Multiwall WS_2 nanotube templates were used as hosts to prepare core–shell PbI_2@WS_2 nanotubes by a capillary-wetting method. Conformal growth of PbI_2 layers on the inner wall of the relatively wide WS_2 nanotubes (i.d. ca. 10 nm) leads to nanotubular structures which were not previously observed in narrow carbon nanotube templates. Image simulation after structural modeling (see picture) showed good agreement with the experimental HRTEM image.

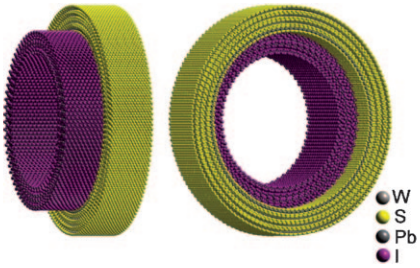

Magnetic Nanoparticles

J.-t. Jang, H. Nah, J.-H. Lee, S. H. Moon, M. G. Kim, J. Cheon* _____ **1234 – 1238**

Critical Enhancements of MRI Contrast and Hyperthermic Effects by Dopant-Controlled Magnetic Nanoparticles

Doped up: The incorporation of Zn^{2+} dopants in tetrahedral sites leads to the successful magnetism tuning of spinel metal ferrite nanoparticles (see picture). $(Zn_{0.4}Mn_{0.6})Fe_2O_4$ nanoparticles exhibit the highest magnetization value among the metal ferrite nanoparticles. Such high magnetism results in the largest MRI contrast effects ($r2 = 860\ mm^{-1}\,s^{-1}$) reported to date and also huge hyperthermic effects.

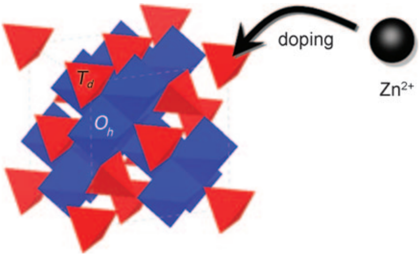

For the USA and Canada: ANGEWANDTE CHEMIE International Edition (ISSN 1433-7851) is published weekly by Wiley-VCH, PO Box 191161, 69451 Weinheim, Germany. Air freight and mailing in the USA by Publications Expediting Inc., 200 Meacham Ave., Elmont, NY 11003. Periodicals postage paid at Jamaica, NY 11431. US POSTMASTER: send address changes to *Angewandte Chemie*, Wiley-VCH, 111 River Street, Hoboken, NJ 07030. Annual subscription price for institutions: US$ 7225/6568 (valid for print and electronic / print or electronic delivery); for individuals who are personal members of a national chemical society prices are available on request. Postage and handling charges included. All prices are subject to local VAT/sales tax.

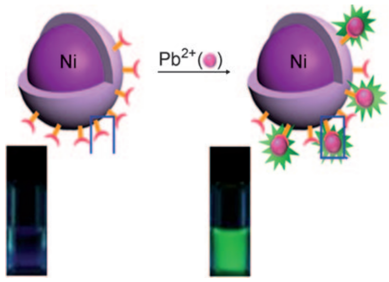

Get the lead out: The title fluorescence receptor exhibits a high affinity and selectivity for Pb^{2+} over competing metal ions in water (see picture) with an overall emission change of approximately 8-fold at the emission maximum for Pb^{2+}. The fluorescence receptor can remove 96 % of 100 ppb Pb^{2+} from human blood, and can be useful and effective for the selective and rapid removal of Pb^{2+} in vivo.

Chemosensors

H. Y. Lee, D. R. Bae, J. C. Park, H. Song, W. S. Han,* J. H. Jung* **1239 – 1243**

A Selective Fluoroionophore Based on BODIPY-functionalized Magnetic Silica Nanoparticles: Removal of Pb^{2+} from Human Blood

---

Let it flow, let it flow: A procedure to generate the first solid-supported mercuric salt, silaphenylmercuric triflate, is described. Silaphenylmercuric triflate showed remarkable catalytic activity for an indole synthesis, furanoyne cyclization, arylyne cyclization, and tandem carbocyclizations. An efficient flow reaction system for indole synthesis and arylyne cyclization is also described (see figure).

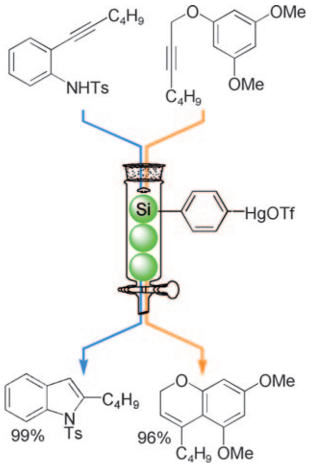

Supported Catalysts

H. Yamamoto,* I. Sasaki, Y. Hirai, K. Namba, H. Imagawa, M. Nishizawa* **1244 – 1247**

Silaphenylmercuric Triflate Catalyzed Reactions: Synthesis of a Solid-Supported Mercuric Salt Catalyst

---

To great (monodisperse) lengths: An improved synthesis of purer ethylene glycol (EG) oligomers allows access to 16- and 32-mers pure enough for multiple incorporation, and also to the longest (48-mer) discrete EG oligomer yet reported. The high purity enables the first crystallizations and hence the first glimpses of secondary 3_{10}-helical PEG structures.

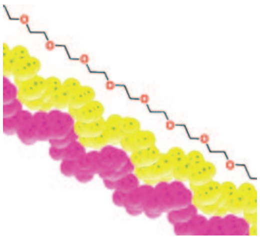

PEG Synthesis

A. C. French, A. L. Thompson, B. G. Davis* **1248 – 1252**

High-Purity Discrete PEG-Oligomer Crystals Allow Structural Insight

---

The natural way: A sensitive NMR spectroscopic method is developed to obtain well-resolved two-dimensional spectra (^{15}N–^{1}H and ^{13}C–^{1}H) for natural-abundance (that is, without the need for isotopic enrichment) large-molecule samples, such as biopharmaceuticals. This method gives structural insights on two lyophilized aprotinin samples and three insulin samples in lyophilized, microcrystalline suspension formulation (red; see picture) and fibril (green) forms.

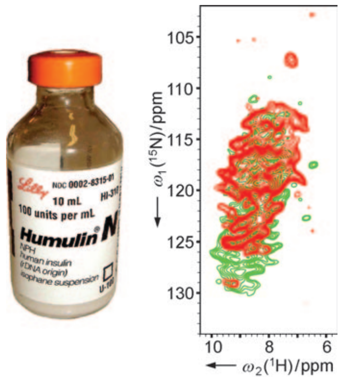

Protein NMR Spectroscopy

D. H. Zhou, G. Shah, C. Mullen, D. Sandoz, C. M. Rienstra* **1253 – 1256**

Proton-Detected Solid-State NMR Spectroscopy of Natural-Abundance Peptide and Protein Pharmaceuticals


A Journal of the Gesellschaft Deutscher Chemiker
Angewandte Chemie
International Edition
GDCh
D 3461
www.angewandte.org
2008–47/16
WILEY-VCH

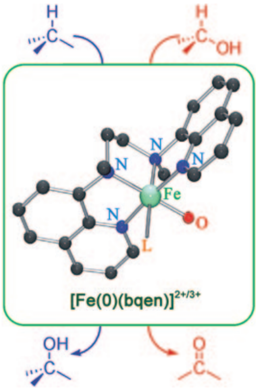

An advanced intermediate: A nonheme iron(IV) oxo complex $[Fe^{IV}(O)(bqen)(L)]^{n+}$ (bqen = *N*,*N*′-dimethyl-*N*,*N*′-bis(8-quinolyl)ethane-1,2-diamine, L = CH_3CN or $CF_3SO_3^-$) activates the C−H bonds of alkanes and alcohols by a hydrogen-atom abstraction mechanism. The catalytic oxidation of these species is proposed to occur through a nonheme iron(V) oxo species, with a high reactivity in oxidation reactions (see picture).

Enzyme Models

J. Yoon, S. A. Wilson, Y. K. Jang, M. S. Seo, K. Nehru, B. Hedman, K. O. Hodgson, E. Bill, E. I. Solomon, W. Nam* ——— **1257 – 1260**

Reactive Intermediates in Oxygenation Reactions with Mononuclear Nonheme Iron Catalysts

---

Heads or tails? The evolution of structural and electronic properties of tin–phthalocyanine films has been analyzed for submonolayer to multilayer coverage using low-temperature scanning tunneling microscopy. Two molecular conformations are observed: randomly dispersed for the first layer, and islands with a single conformation in subsequent layers.

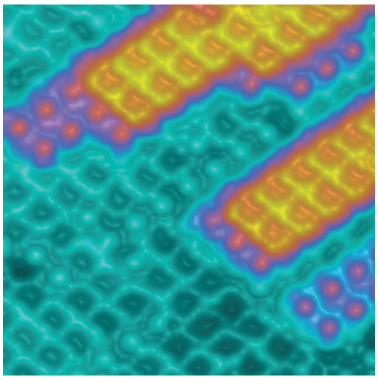

Organic–Inorganic Hybrids

Y. Wang, J. Kröger,* R. Berndt, W. Hofer ——— **1261 – 1265**

Structural and Electronic Properties of Ultrathin Tin–Phthalocyanine Films on Ag(111) at the Single-Molecule Level

---

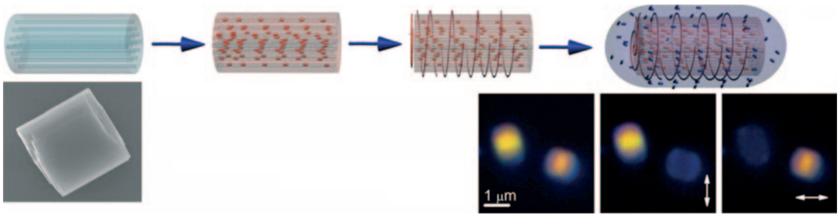

Multicolor fluorescent containers: A silica coating procedure has been devised for the preparation of multifluorescent dye-loaded zeolite L crystals with luminescent anisotropic cores and isotropic shells. The method comprises a combination of the polyelectrolyte layer-by-layer technique and Stöber synthesis (see scheme, TEM image, and fluorescence microscopy images).

Core–Shell Materials

A. Guerrero-Martínez,* S. Fibikar, I. Pastoriza-Santos, L. M. Liz-Marzán, L. De Cola* ——— **1266 – 1270**

Microcontainers with Fluorescent Anisotropic Zeolite L Cores and Isotropic Silica Shells

---

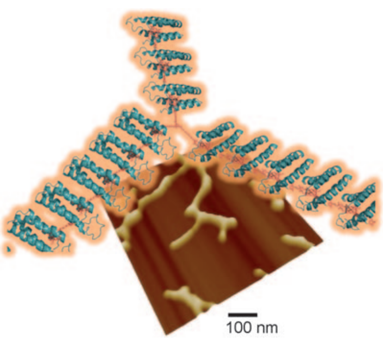

Supramolecular protein polymers: When a heme moiety was introduced to the surface of an apo-cytochrome b_{562}(H63C) mutant, supramolecular polymers formed through noncovalent heme–heme pocket interactions. The incorporation of a heme triad as a pivot molecule in the protein polymer further led to a two-dimensional protein network structure, which was visualized by tapping-mode atomic force microscopy (see picture).

Protein Self-Assembly

H. Kitagishi, Y. Kakikura, H. Yamaguchi, K. Oohora, A. Harada, T. Hayashi* ——— **1271 – 1274**

Self-Assembly of One- and Two-Dimensional Hemoprotein Systems by Polymerization through Heme–Heme Pocket Interactions

Contents

Supramolecular Chemistry

C. Park, K. Lee, C. Kim* ___ **1275 – 1278**

Photoresponsive Cyclodextrin-Covered Nanocontainers and Their Sol-Gel Transition Induced by Molecular Recognition

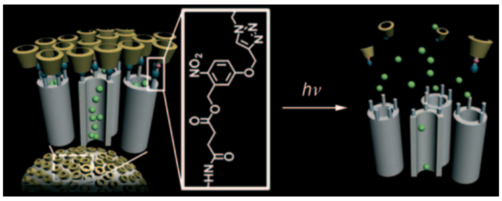

Springing the trap: Cyclodextrin-covered mesoporous silica nanoparticles with photocleavable linkers exhibit photoinduced release characteristics and a sol–gel transition that is induced by molecular recognition (see picture). Upon exposure to UV light, the guest molecules were released from the pore by removal of the CD “gatekeeper”, which was linked on the surface of the silica nanoparticle through a photocleavable *o*-nitrobenzyl ester moiety.

Asymmetric Catalysis

C. Zhong, Y. Chen, J. L. Petersen, N. G. Akhmedov, X. Shi* ___ **1279 – 1282**

Enantioselective Intermolecular Crossed-Conjugate Additions between Nitroalkenes and α,β-Enals through a Dual Activation Strategy

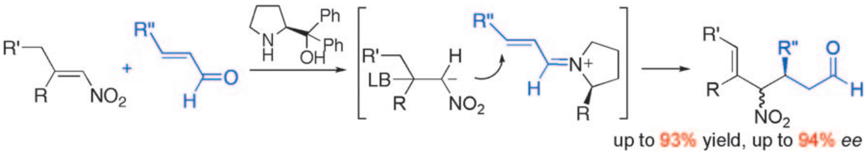

Double the fun: The title reaction was developed by using a Lewis base/iminium activation strategy (see scheme). The reaction proceeded with excellent yields and *ee* values, and the products were additionally transformed into a single enantiomer of a substituted pyrrolidine with excellent retention of configuration.

Natural Products

X. Wu, J. Zhou, B. B. Snider* ___ **1283 – 1286**

Synthesis of (−)-Berkelic Acid

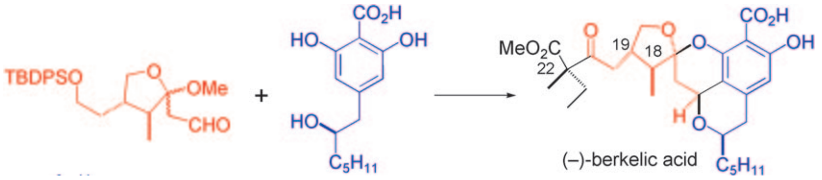

An extremophilic challenge: Stereospecific condensation of a fully functionalized ketal aldehyde and a 2,6-dihydroxybenzoic acid is the key step in the synthesis of (−)-berkelic acid confirming Fürstner’s reassignment of the stereochemistry at C18 and C19, establishing the absolute stereochemistry, and tentatively assigning the stereochemistry at C22.

Asymmetric Synthesis

M. Vasylyev, H. Alper* ___ **1287 – 1290**

Diastereoselective Synthesis of Hexahydropyrrolo[2,1-*b*]oxazoles by a Rhodium-Catalyzed Hydroformylation / Silica-Promoted Deformylation Sequence

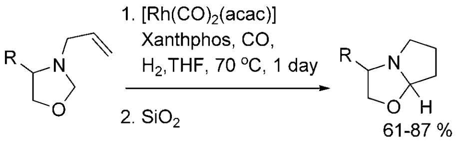

Fleetingly formyl: A new rhodium-catalyzed hydroformylation reaction of *N*-allyl oxazolidines, carried out under a CO/H_2 atmosphere, followed by a diastereoselective deformylative cyclization affords hexahydropyrrolo[2,1-*b*]oxazoles in good yields. The reaction proceeds by a unique hydroformylation–deformylation sequence in which the formyl group virtually substitutes for the {CH_2–O} fragment of the oxazolidine heterocycle.

Isotope Effects

E. J. Klinker, S. Shaik,* H. Hirao,
L. Que, Jr.* ______ 1291 – 1295

A Two-State Reactivity Model Explains Unusual Kinetic Isotope Effect Patterns in C–H Bond Cleavage by Nonheme Oxoiron(IV) Complexes

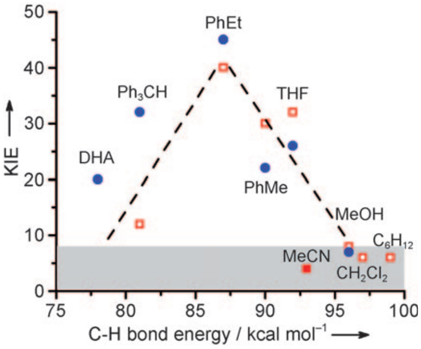

It's in the bond: The cleavage of C–H bonds by two related oxoiron(IV) complexes shows a range of kinetic isotope effect (KIE) values that exhibit an unusual dependence on the C–H bond strength. Large nonclassical KIEs are observed for bond strengths below 93 kcal mol^{-1}, while semiclassical values are found above this value (see graph, DHA = 9,10-dihydroanthracene). This nonintuitive behavior can be rationalized by invoking a two-state reactivity model.

Tsuji–Trost Allylations

A. Hazari, V. Gouverneur,*
J. M. Brown* ______ 1296 – 1299

Palladium-Catalyzed Substitution of Allylic Fluorides

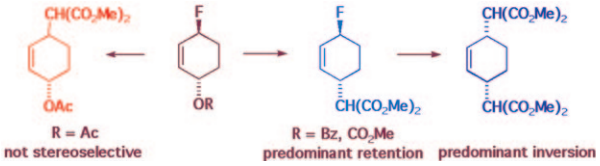

As unusual substrates for the Tsuji–Trost allylation reaction, allylic fluorides are responsive to palladium-catalyzed substitution. Their activity towards this reaction fits in the series OCO$_2$Me > OBz ≫ **F** ≫ OAc. The classic stereoretention mechanism that involves sequential inversions does not operate in this case. Several distinct cases are considered.

Enzyme Inhibitors

K. A. Stubbs,* M. S. Macauley,
D. J. Vocadlo* ______ 1300 – 1303

A Selective Inhibitor Gal-PUGNAc of Human Lysosomal β-Hexosaminidases Modulates Levels of the Ganglioside GM2 in Neuroblastoma Cells

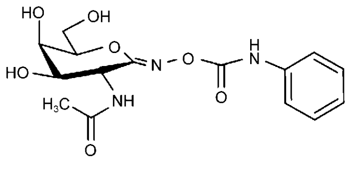

Gal-PUGNAc

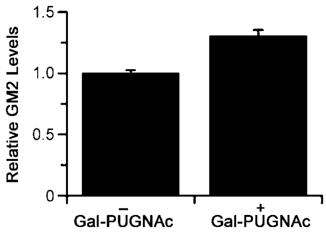

Gal-PUGNAc (see picture), a highly selective inhibitor for β-hexosaminidases HEXA and HEXB is cell-permeable and modulates the activity of HEXA and HEXB in tissue culture, increasing ganglioside GM2 levels. Gal-PUGNAc should allow the role of these enzymes to be studied at the cellular level without generating a complex chemical phenotype from concomitant inhibition of *O*-GlcNAcase.

Domino Reactions

H. Ishikawa, T. Suzuki,
Y. Hayashi* ______ 1304 – 1307

High-Yielding Synthesis of the Anti-Influenza Neuramidase Inhibitor (−)-Oseltamivir by Three "One-Pot" Operations

Taking shortcuts: A remarkably short and high-yielding asymmetric total synthesis of (−)-oseltamivir takes advantage of organocatalysis and single-pot domino operations. The target, known as the drug Tamiflu, is prepared efficiently in a short time, and also its derivatives can be synthesized effectively.

Nucleation

T. H. Zhang, X. Y. Liu* ______ **1308 – 1312**

Nucleation: What Happens at the Initial Stage?

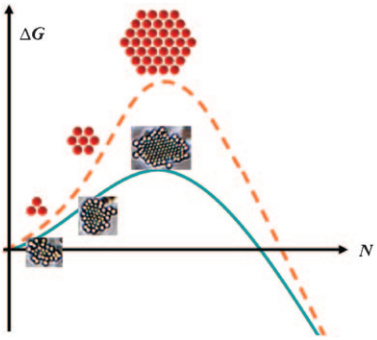

Crystallizing growth: The initial structure of crystal nuclei is supersaturation-dependent. At low degrees of supersaturation, liquid-like nuclei are formed initially, which undergo a continuous structure transition from liquid-like to crystal-like as the size N increases. This gradual structure evolution substantially lowers the nucleation barrier ΔG^* and facilitates the nucleation relative to the formation of crystal-like clusters from the beginning.

Organocatalysis

P. G. Cozzi,* F. Benfatti,
L. Zoli ______ **1313 – 1316**

Organocatalytic Asymmetric Alkylation of Aldehydes by S_N1-Type Reaction of Alcohols

Work-alcoholic! The elusive enantioselective catalytic α-alkylation of aldehydes, a widely sought transformation, was brought to execution by the use of alcohols capable of forming stabilized carbocations (see scheme, TFA = trifluoroacetic acid).

Natural Product Synthesis

A. Boyer, G. E. Veitch, E. Beckmann,
S. V. Ley* ______ **1317 – 1320**

Second-Generation Synthesis of Azadirachtin: A Concise Preparation of the Propargylic Mesylate Fragment

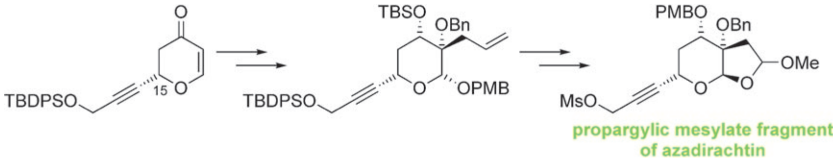

A second bite of the apple: A new and highly efficient synthesis of the propargylic mesylate fragment of azadirachtin has been accomplished (see scheme; Bn = benzyl, Ms = methanesulfonyl, PMB = *para*-methoxybenzyl, TBDPS = *tert*-butyldiphenylsilyl). An enantioselective catalytic hetero Diels–Alder reaction sets up the stereocenter at C15, which then controls the installation of the remaining functionality in a total of only 17 steps.

Mass Spectrometry

Z. Tian, S. R. Kass* ______ **1321 – 1323**

Gas-Phase versus Liquid-Phase Structures by Electrospray Ionization Mass Spectrometry

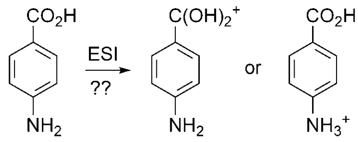

Preferred protonation: Does electrospray ionization mass spectrometry produce gas-phase or liquid-phase structures? The preferred protonation site in *p*-aminobenzoic acid depends upon the medium, and the structure of its conjugate acid varies with the solvent used during spraying.

Catalytic Hydrogenation

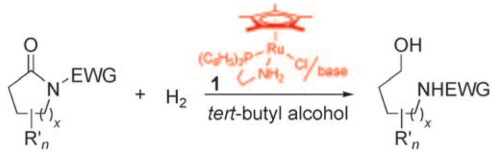

Awakening of the Cp one: The bifunctional complex **1** facilitates the interaction with substrates bearing less electrophilic carbon atoms than ketones, epoxides, and imides. The title reaction was applicable to the reduction of Evans' asymmetric alkylation products to the chiral alcohols along with good recovery of the chiral oxazolidinone auxiliary. EWG = electron-withdrawing group.

Aziridinium Salts

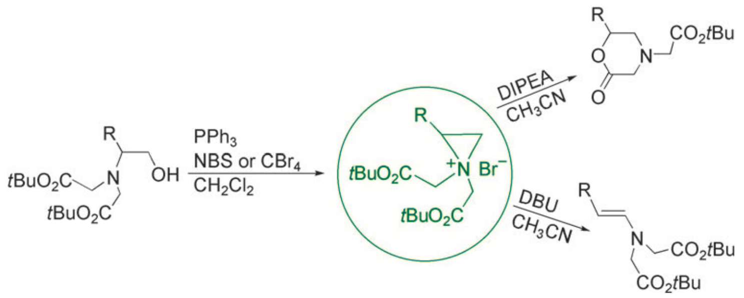

Rock trapping and exploration: Aziridinium bromide salts were discovered serendipitously during bromination of *N*,*N*-dicarboxymethylated β-amino alcohols. Regiospecific ring-opening and rearrangement of the isolated, surprisingly stable aziridinium salts produces useful molecules including C-functionalized oxomorpholines and α,β-unsaturated amines.

Supporting information is available on www.angewandte.org (see article for access details).

A video clip is available as Supporting Information on www.angewandte.org (see article for access details).

Service